Supplementary Information (SI) for Soft Matter.

Supporting Information: Micro-Ballistic Response of Thin Film Polymer Grafted Nanoparticle Monolayers

Subhadeep Pal[†] and Sinan Keten[*,†,‡]

†*Department of Civil and Environmental Engineering, Northwestern University, Evanston, IL, USA*

‡*Department of Mechanical Engineering, Northwestern University, Evanston, IL, USA*

E-mail: s-keten@northwestern.edu

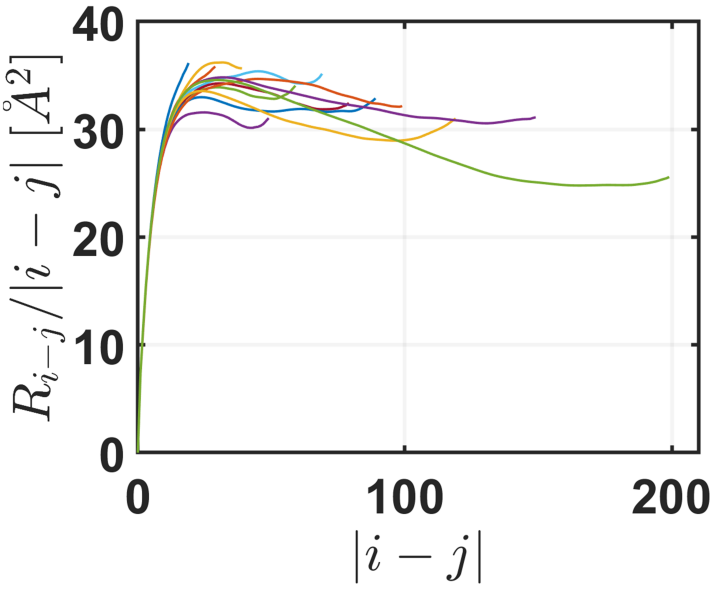

Figure S1: Mean squared internal distance for PGNs at different graft lengths indicated by distinct colors.

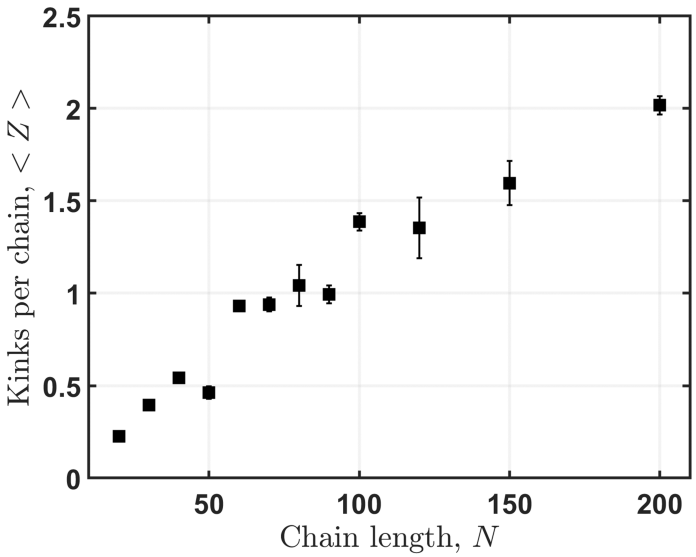

Figure S2: Number of kinks per chain with increasing graft length calculated with Z1+ algorithm. A value more than 1 indicates entanglement in the system. The error bar represents the standard deviation from three different trials.

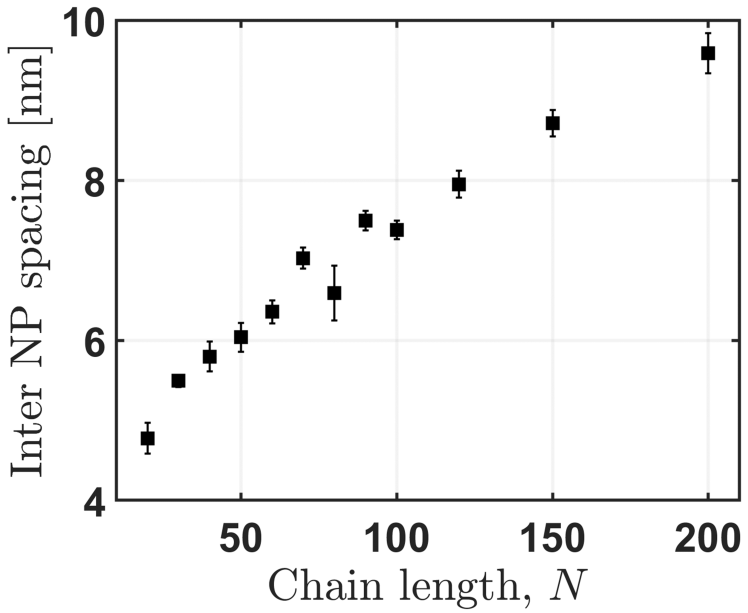

Figure S3: The change of spacing between nanoparticles with increasing graft length. The error bar represents the standard deviation from three different trials.

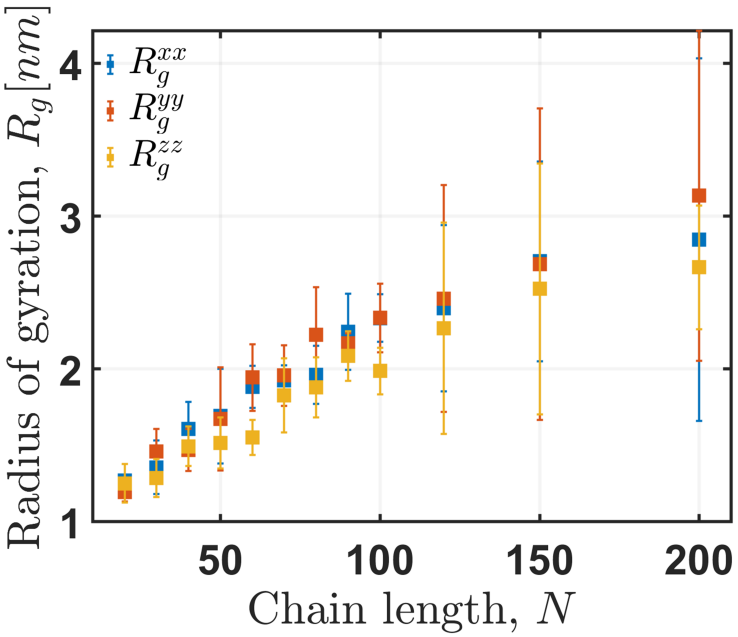

Figure S4: Radius of gyration in three principle directions, R_g^{xx}, R_g^{yy}, and R_g^{zz}. The value of R_g^{zz} is slightly lower than the other two because of the free surface effect. However, all components of R_g increase as the graft length becomes longer. The error bar represents the standard deviation from three different trials.

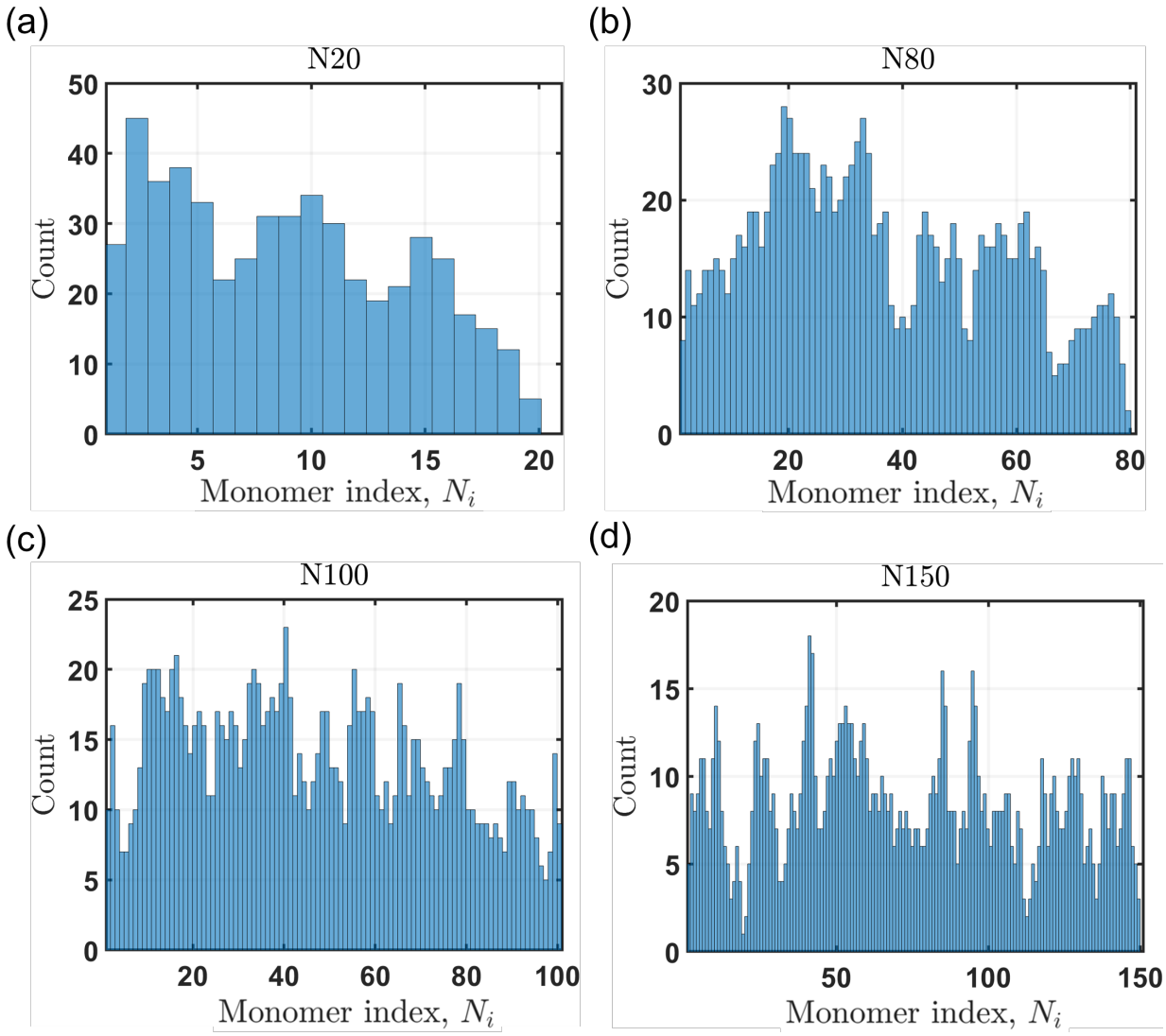

Figure S5: Number of backbone bonds broken with monomer index, N_i, in SiO_2-PGNs with N20, N80, N100, and N150 grafts.

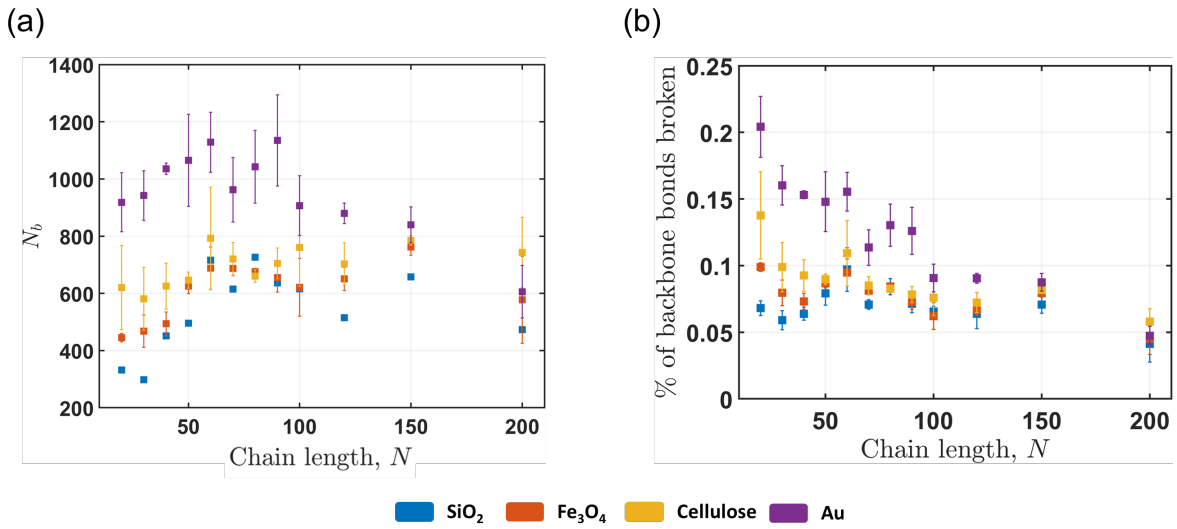

Figure S6: (a) Number (N_b) and (b) percentage of backbone bond scission events with varying graft length and different NP cores. Bond scission percentage increases with increasing graft length and heavier NP cores, due to hindered chain slippage in the former and inertial effects in the latter.

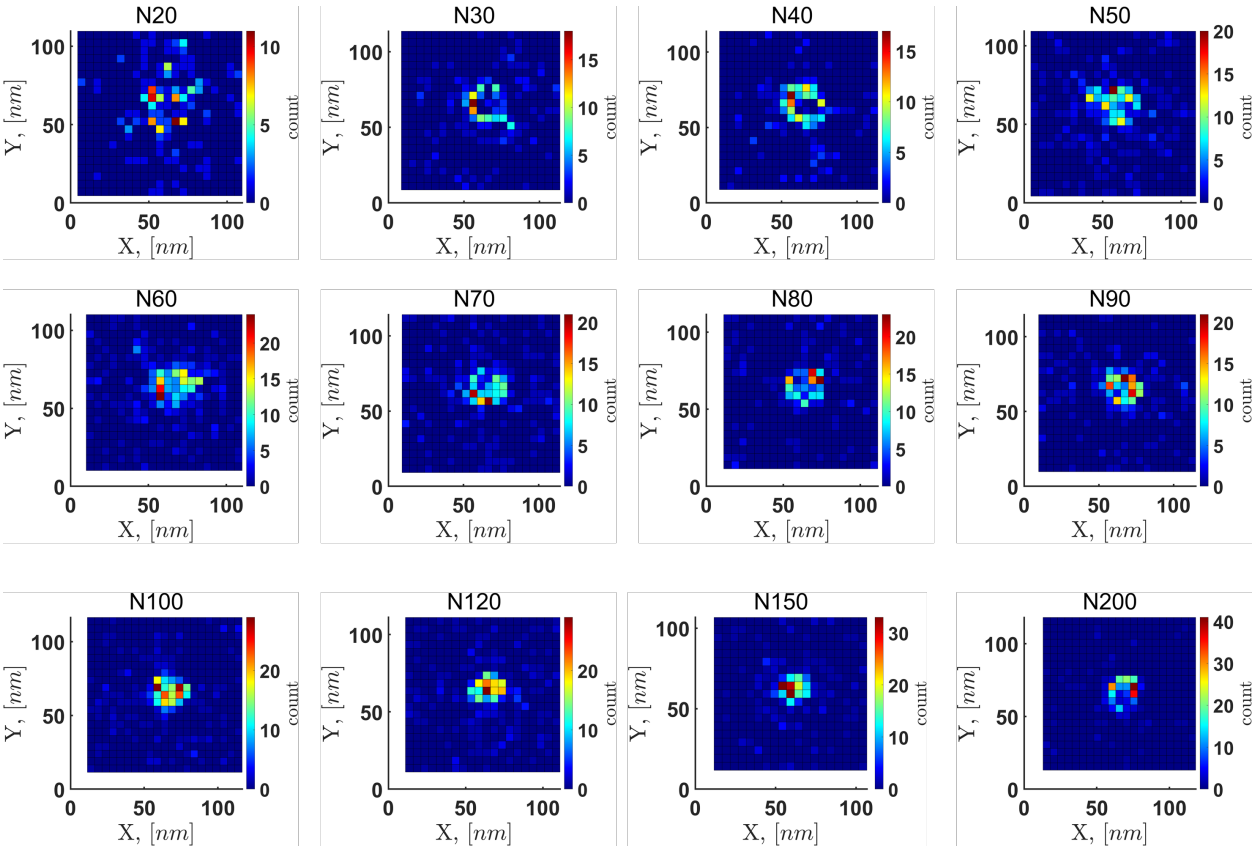

Figure S7: Spatial distribution of bond scission location for different graft lengths in SiO_2 core PGNs. The mid-point indicates the point of bullet impact. The scission mainly occurs around the impact region. For PGNs with shorter grafts, events are slightly scattered as the NP core can move more easily.

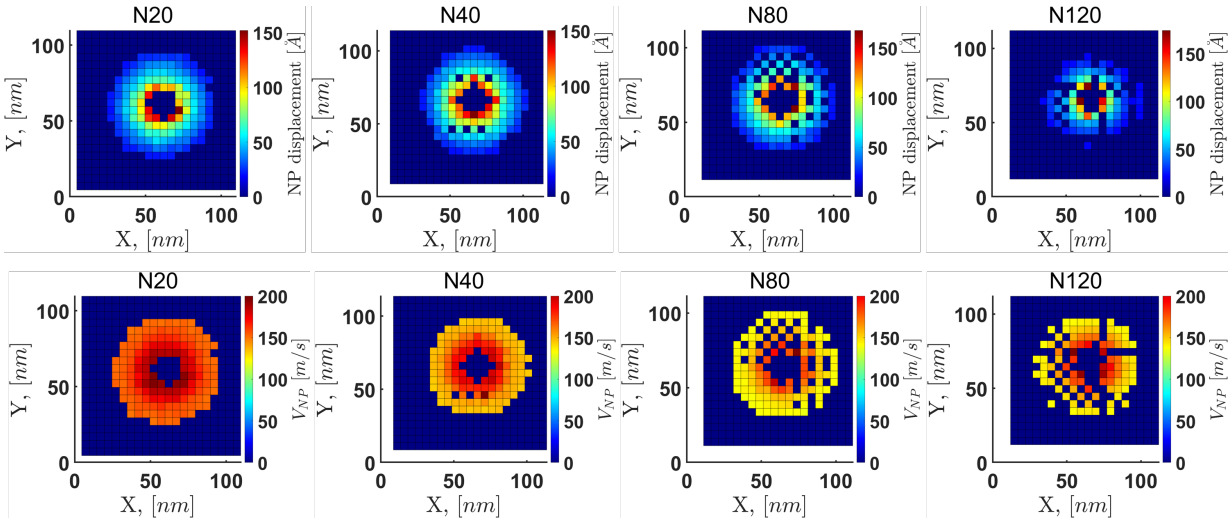

Figure S8: Spatial distribution of NP core location for four different graft lengths in *Cellulose* PGNs. The color shows the average NP displacement and velocity in that grid for the top and bottom panels, respectively. Both the displacement and velocity radially decrease from the impact zone. NP cores with longer grafts exhibit small displacements. However, the velocity, V_{NP} stays almost constant in different grafts. The displacement and velocity patterns do not match because the velocities are instantaneous values taken from three snapshots around when the bullet passes through the film.

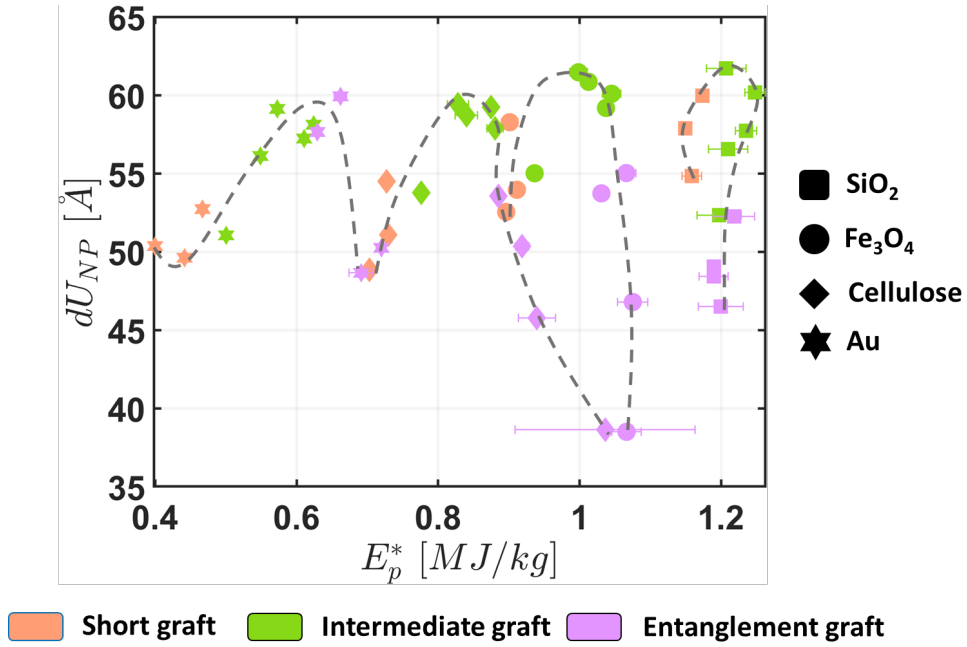

Figure S9: Average NP core displacement (dU_{NP}) vs specific penetration energy (E_p^*). Different colors and shapes indicate various graft lengths and NP core types. For every NP core type, dU_{NP} increases in the intermediate graft regime. Splines are fitted to guide the eye.

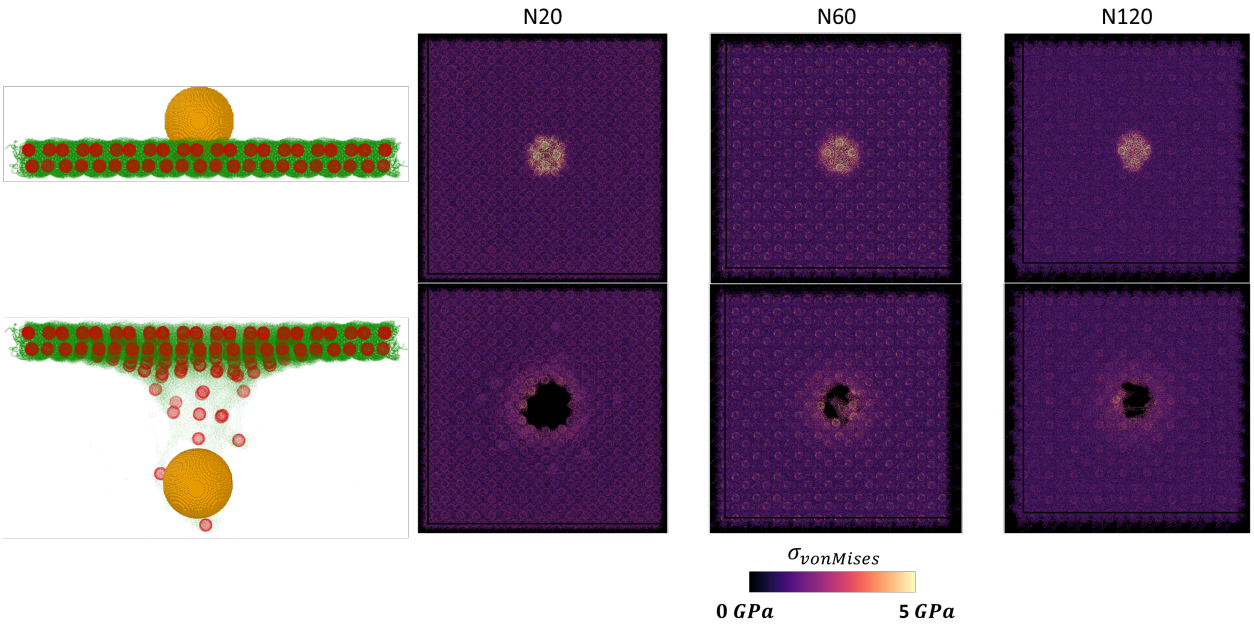

Figure S10: vonMises ($\sigma_{vonMises}$) stress contours in N = 20, 60, and 120 grafts with Fe_3O_4 NP core. The top row panels show $\sigma_{vonMises}$ when the bullet touches the film (top view), and the bottom row panels are when the bullet passes through the film (bottom view).

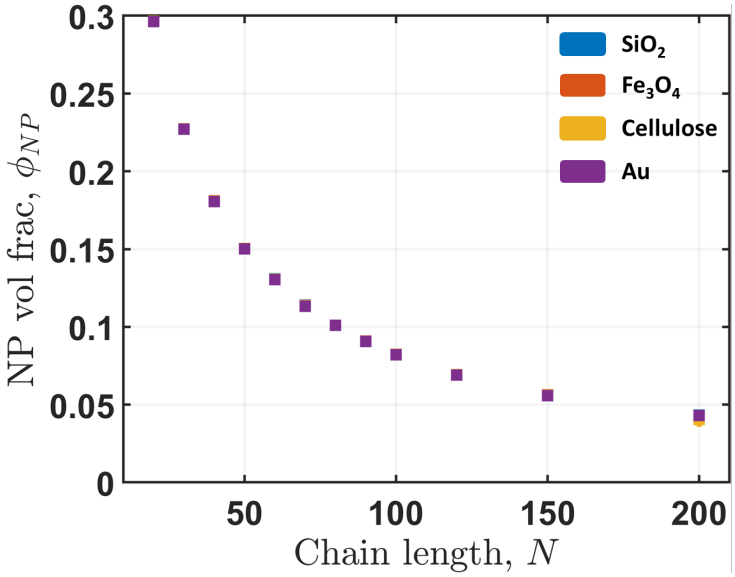

Figure S11: Change of NP volume fraction, ϕ_{NP} with grafted chain lengths for different NP core types. The ϕ_{NP} is exactly the same for all core types since only density is changed.

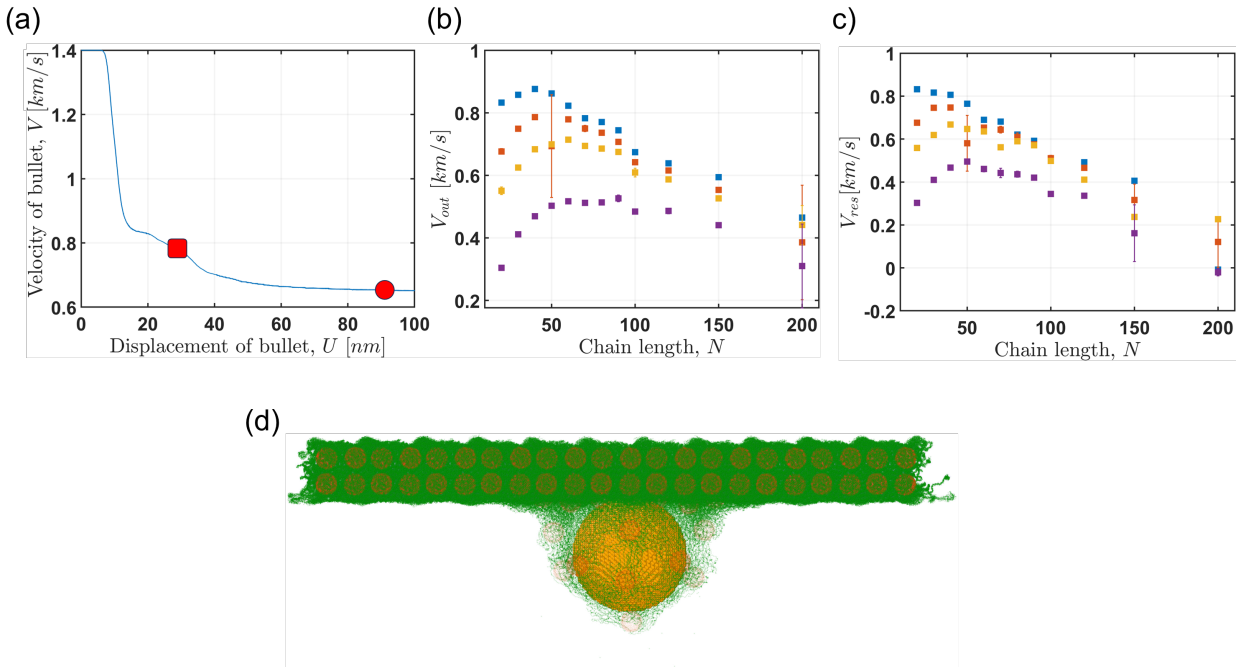

Figure S12: (a) Change of bullet velocity with displacement during the ballistic simulation in Fe_3O_4 PGN with $N = 60$. The trend of (b) V_{out}, and (c) V_{res} for different NP core and graft lengths. (d) Snapshot from Fe_3O_4 PGN with $N = 60$ right after the bullet passes through the film, and V_{out} is computed around this time. The V_{res} is calculated when bullet's deceleration become almost zero. The circular and square markers in (a) indicate V_{res} and V_{out}, respectively. Both V_{out} and V_{res} are higher for lighter cores and reduce when grafted chains become longer.

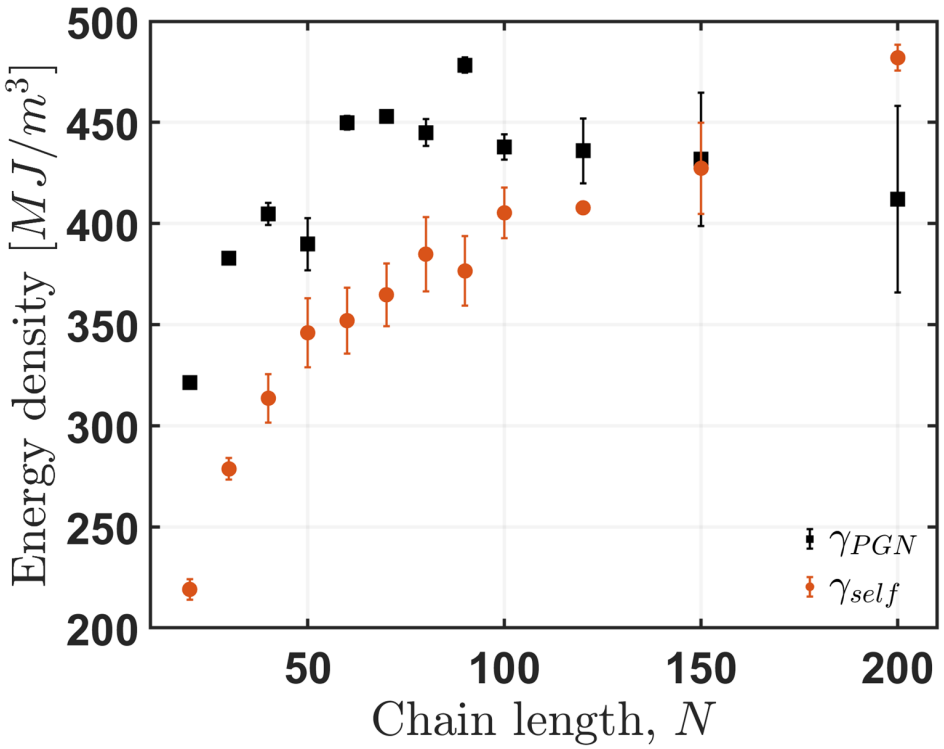

Figure S13: Change of volume normalized PGN cohesive energy density (γ_{PGN}), and PGN self interaction energy density (γ_{self}) with increasing graft length. γ_{self} indicates the intra-PGN interaction, which increases with chain length and crosses inter-PGN energy (γ_{PGN}) as the chain starts to entangle.

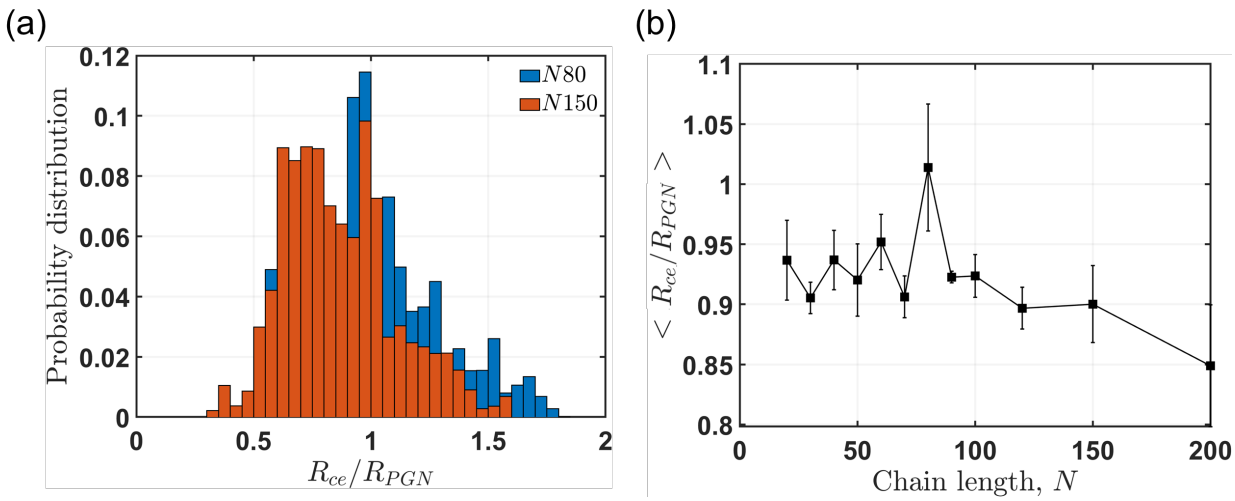

Figure S14: (a) Probability distribution of polymer's end distances from the PGN center normalized by inter PGN distance, R_{ce}/R_{PGN} for graft length $N = 80$, and 150 in PGNs with Au core. In both PGNs, polymer grafts extend to their next nearest neighbors ($Rce/R_{PGN} > \sqrt{2}$). (b) The trend of $< R_{ce}/R_{PGN} >$, which changes slightly with varying graft length.

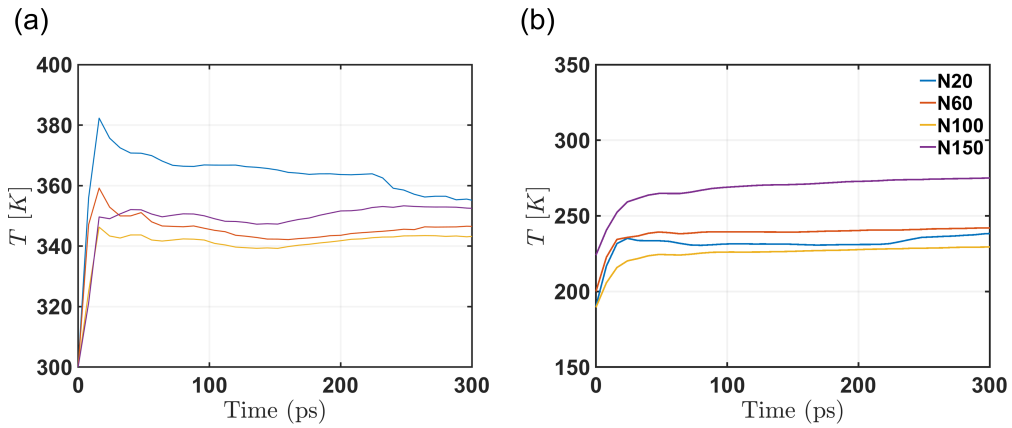

Figure S15: Variation of thin film temperature during micro-ballistic simulation considering (a) all velocity components (v_x, v_y, and v_z), and (b) only two components (v_x, and v_y). The v_z is neglected to check film temperature without the effect of downward movement.

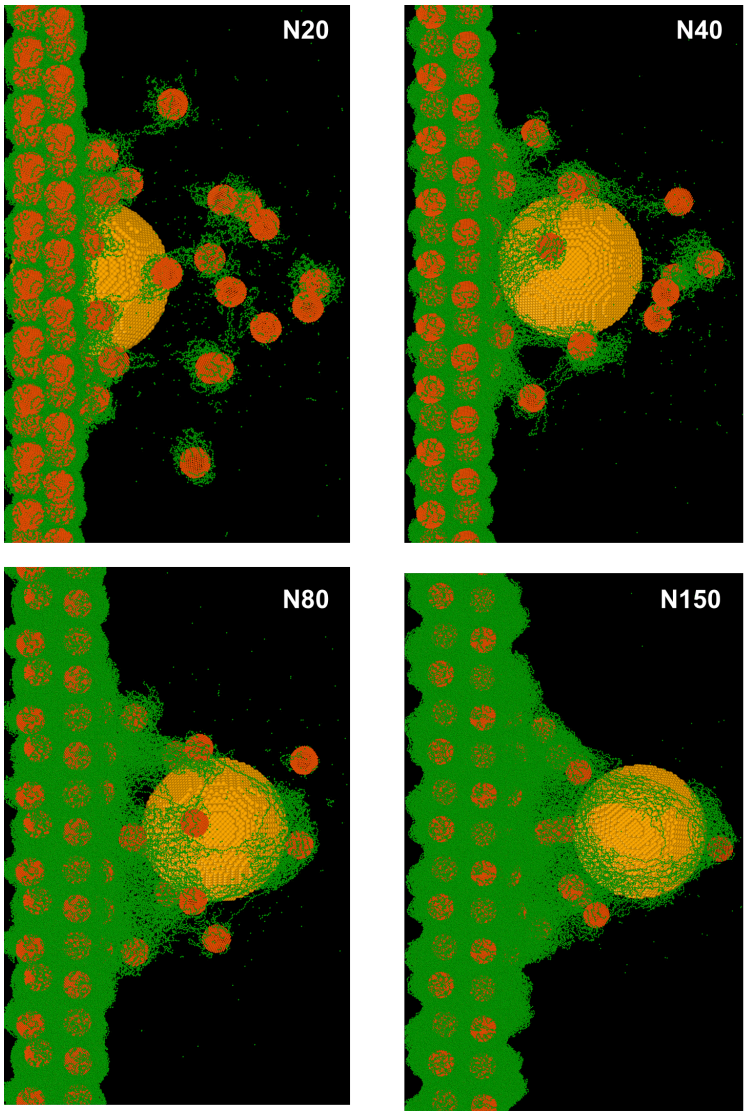

Figure S16: Failure snapshots of Au PGNs with (a) $N = 20$, (b) $N = 40$, (c) $N = 80$, and (d) $N = 150$. The color indicates different beads: green - polymer, red - NP core, and yellow - bullet.

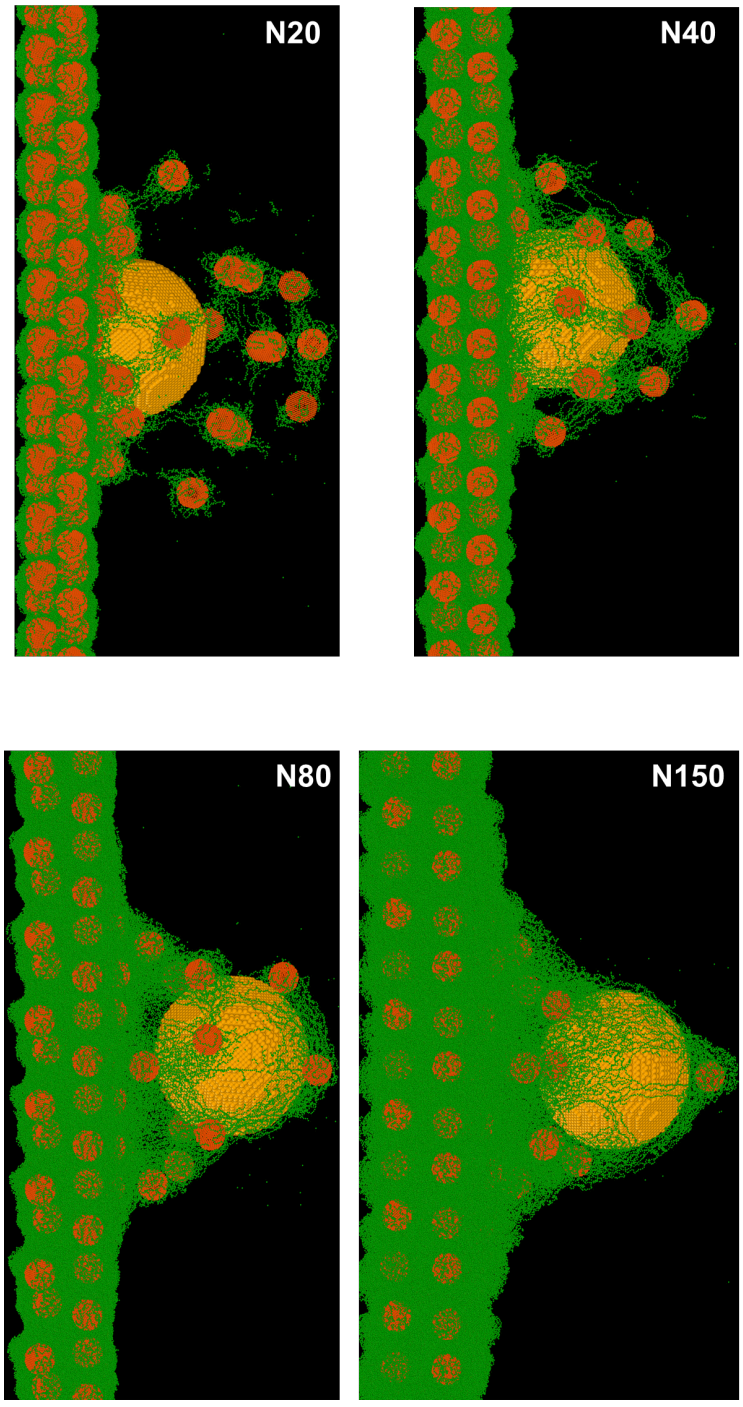

Figure S17: Failure snapshots of *Cellulose* PGNs with (a) $N = 20$, (b) $N = 40$, (c) $N = 80$, and (d) $N = 150$. The color indicates different beads: green - polymer, red - NP core, and yellow - bullet.

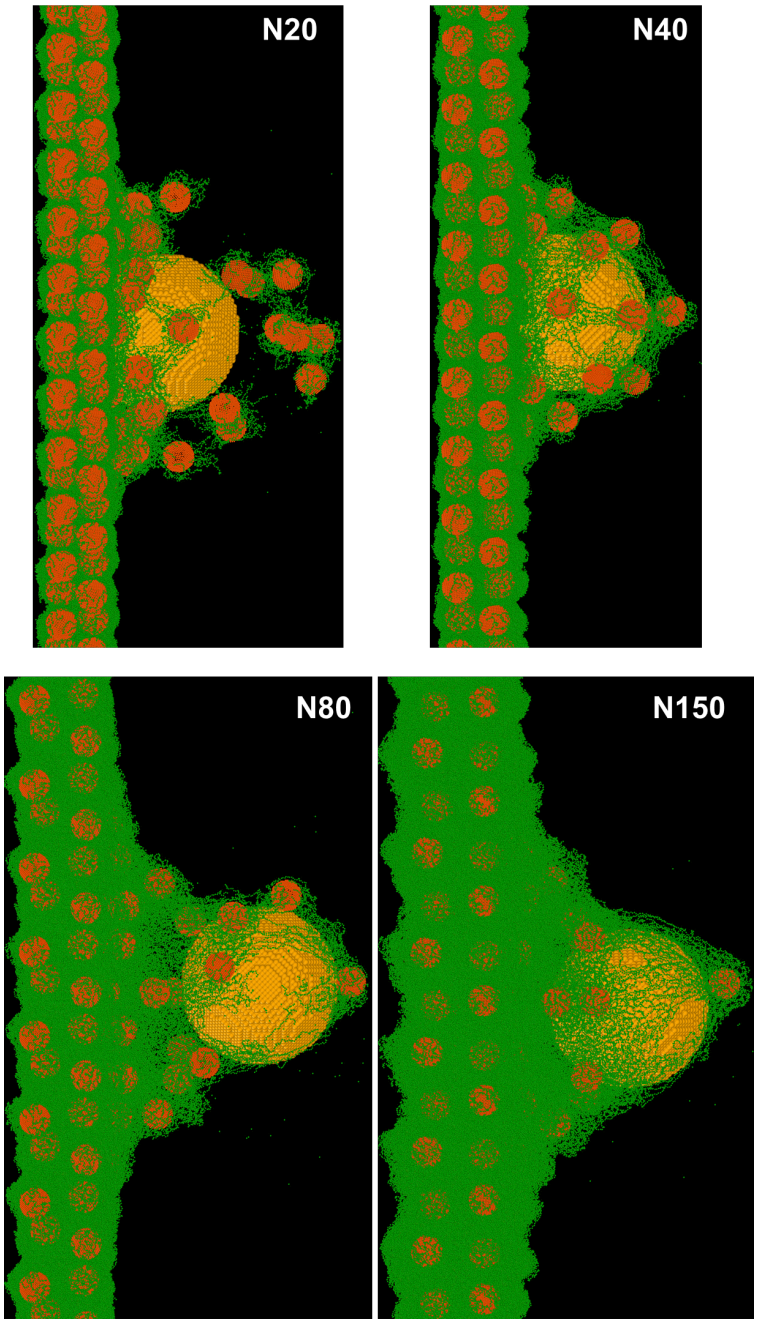

Figure S18: Failure snapshots of SiO_2 PGNs with (a) $N = 20$, (b) $N = 40$, (c) $N = 80$, and (d) $N = 150$. The color indicates different beads: green - polymer, red - NP core, and yellow - bullet.